New compounds and structures in the solid state

Edmund J. Cussen
DOI: 10.1039/b716500p

This chapter reviews the 2007 literature on new compounds and structures in the solid state.

Highlights

Many of the highlights of solid state chemistry that were reported in the literature during 2007 arise from studies of structures of surprising simplicity or else from astonishingly complex problems that are at the limits of the analytical techniques. A striking example of the former is the report of the binary compound ReB_2 that can be prepared by direct combination of the elements in a sealed tube. The hardness of this apparently simple material is second only to diamond. Similarly the rutile structure of TcO_2 has been described for the first time and an important chemical consideration of the effect cation doping of Zintl phases has been described. The use of topotactic modification has yielded many new mixed-metal oxides and chalcogenides of increasing complexity, with several new anion- or cation-ordering schemes being observed, as well as stabilising the remarkable perovskite-related phase $SrFeO_2$. Complexity has also been a feature of both intermetallic phases and zeolites. The former are exemplified by the $>33\,000$ Å^3 unit cell volume of a new phase in the Li/Na/Ba system whilst the latter are represented by the 24-topologically distinct Si atoms observed in the structure of the industrially-important zeolite IM-5.

1. Oxides

The β-emitter ^{99}Tc is a long-lived isotope but despite a half life of 2.12×10^5 years the oxide chemistry of technetium has been relatively neglected and the crystal structure of the black binary phase TcO_2 has not previously been reported. Neutron powder diffraction has been employed to complement existing X-ray absorption studies of this compound. Thus the last unknown structure of a simple transition metal oxide has been identified as possessing a distorted rutile arrangement.[1] This compound crystallises in the space group $P2_1/c$ with lattice parameters (a = 5.6891(1), b = 4.7546(1), c = 5.5195(1) Å and β = 121.453(1)°) in reasonable agreement with a previous indexing of X-ray diffraction data. The rarity of structural studies of technetium compounds is illustrated by necessity of improving the estimated neutron scattering length of ^{99}Tc from 6.8 fm to 6.00(3) fm. The distortion of the structure is largely invariant at temperatures down to 15 K and arises from Tc–Tc bonding between the edge-sharing TcO_6 octahedra in the

WestCHEM, Department of Pure and Applied Chemistry, The University of Strathclyde, Glasgow, Scotland, UK G12 8PT. E-mail: Edmund.Cussen@Strath.ac.uk; Fax: +44 141 548 4822; Tel: +44 141 548 2797

structure. The bonding is significantly weaker than that found in the related compounds MoO_2 and WO_2. Metal–metal interactions are also a key feature in the structure of $La_3Re_2O_{10}$ with an Re···Re separation between edge sharing ReO_6 octahedra of 2.488 Å indicating an Re–Re interaction with a bond order of 1.5. Neutron diffraction has been used to study a bulk, polycrystalline sample for the first time[2] and confirmed the structure previously assigned from a single crystal study as containing $[Re_2O_{10}]^{9-}$ dimers separated by La^{3+} cations. The mean oxidation state of $Rh^{5.5+}$ indicates each dimer must have at least one unpaired electron and calculations show that this is extensively delocalised over all twelve atoms in the cluster with surprisingly strong magnetic interactions between these dimer units, although a magnetic structure could not be determined, presumably due to the delocalised nature of the magnetic moment.

Structural studies of the effects of nickel doping of $Mg_4Nb_2O_9$ are of importance due to the attractive microwave dielectric properties of these compositions. The corundum-related phase of the undoped compound ($x = 0$) is preserved in the series $Mg_{4-x}Ni_xNb_2O_9$ ($0 \leq x \leq 2.75$) whilst compositions in the range $2.75 \leq x \leq 4$ are isostructural with II-$Ni_4Nb_2O_9$.[3] These structures are both closely related to corundum, and contain layers of Mg and Ni alternating with double layers composed of Mg, Ni and Nb. The difference in these structures arises from the filling patterns within these layers with the magnesium-rich compounds containing isolated vacant sites whilst the nickel-rich structure contains these vacancies in chains. These arrangement lead to the distinctive honeycomb and chain patterns shown in Fig. 1. A careful transmission electron microscopy study of $MgNi_3Nb_2O_9$ has identified defects in this structure that suggest that alternative cation-ordering schemes are possible in the corundum structure and that stabilising these in bulk phases may lead to the formation of new materials.

Unusual cation ordering has also been reported in a series of perovskite-related compounds $KLaMnWO_6$, $NaLnMnWO_6$ (*Ln* = La, Nd, Tb) and $NaNdMWO_6$ (*M* = Co and Mg).[4] Each of these compounds contain W^{6+} and the divalent cation in a rock-salt arrangement over the octahedral sites in the structure in a manner commonly observed in perovskites. However, these compounds are highly unusual in also containing an ordered arrangement of K^+ or Na^+ and Ln^{3+} over layers in the structure. These compounds contain complex tilting arrangements of the oxide

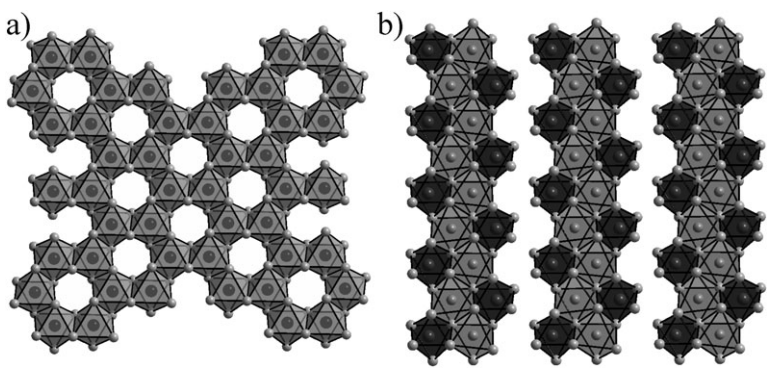

Fig. 1 The phase $Mg_3NiNb_2O_9$ contains (a) honeycomb of edge-sharing (Mg, Ni)O_6 units shown as light grey octahedra. In addition to the honeycomb arrangement $MgNi_3Nb_2O_9$ also contains chains of (Mg, Ni)O_6 octahedra linked to NbO_6 shown as dark grey units.[3]

octahedra which, in the case of $NaLaMnWO_6$, $NaNdMnWO_6$ and $NaTbMnWO_6$ lead to crystallisation in the non-centrosymmetric space group $P2_1$. The cation ordering is stabilised by the displacement of the d^0 cation W^{6+} from the centre of the octahedron, towards the layer containing Na^+. Combined with the presence of paramagnetic Mn^{2+} and reasonably strong magnetic interactions these structural features suggest that this cation-ordering scheme may provide a route to new multiferroic compounds. Where the octahedral sites of the perovskite structure are occupied in a 3:1 ratio an unusual ordering scheme can develop. In the case of $Ba_{4-x}Sr_xNaSb_3O_{12}$ the octahedral sites are populated such that metal-oxide chains containing an alternating arrangement of Na^+ and Sb^{5+} are themselves arranged in an alternating fashion with chains composed entirely of SbO_6 octahedra as shown in Fig. 2. For the $x = 0$ composition $Ba_4NaSb_3O_6$ the resulting cubic phase provides a rare example of a perovskite containing no tilting of the octahedra. Replacement of Ba^{2+} with the smaller Sr^{2+} cation leads to the progressive introduction of octahedral tilting and the reduction in symmetry from cubic ($Im\bar{3}m$) through tetragonal ($P4/mnc$) and orthorhombic (Cmca) to the monoclinic space group $P2_1/n$.[5] This is the first time that tilting in such a 3:1 cation-ordered phase has been found.

A similar approach has been employed to reduce the symmetry of 1:1 ordered compounds $Ba_{2-x}Sr_xErMoO_6$ from cubic ($Fm\bar{3}m$) through tetragonal ($I4/m$) to monoclinic ($P2_1/n$) in an unsuccessful attempt to stabilise a Jahn–Teller distortion in the MoO_6 octahedron.[6] The same rock salt ordering motif is observed between Cr^{3+} and Sb^{5+} in the perovskites Ca_2CrSbO_6 and Sr_2CrSbO_6.[7] Related chromium-containing compounds show exceptionally high magnetic ordering temperatures, but these materials show magnetic ordering at 12 K and 16 K to give antiferromagnetic and ferromagnetic states for Sr_2CrSbO_6 and Ca_2CrSbO_6, respectively. The latter is the first example of a ferromagnetic double perovskite containing only one paramagnetic species on the six-coordinate site. Both compounds adopt the same tilting scheme of the oxide octahedra and the increase in this structural distortion on replacing Sr^{2+} with Ca^{2+} increases the strength of the ferromagnetic exchange

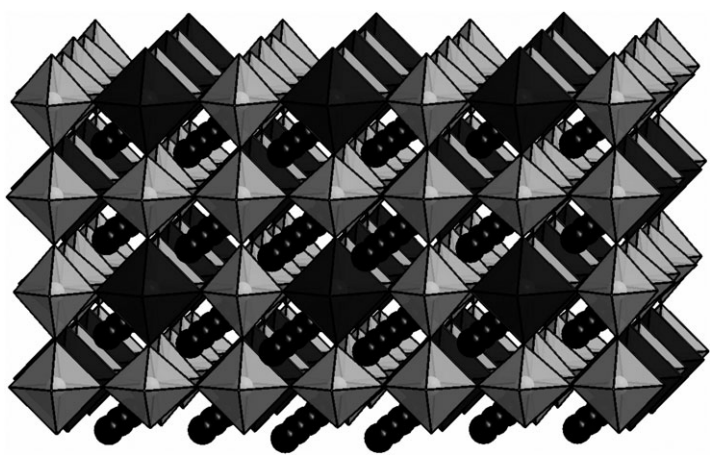

Fig. 2 The cubic structure of $Ba_4NaSb_3O_{12}$ contains NaO_6 and SbO_6 units (represented by grey and black octahedra, respectively). The structure is built up from chains of alternating NaO_6 and SbO_6 that alternate with chains composed exclusively of SbO_6 octahedra. Ba cations are shown as black spheres.[5]

relative to the competing antiferromagnetic interaction to give a ferromagnetically ordered moment of 2.6(2) μ_B per Cr^{3+}. The same tilt system has been reported for the new phases Sr_2MUO_6 (M = Mn, Fe, Ni and Zn).[8] The crystallographic structures of these compounds suggest that the oxidation states are intermediate between the M^{2+}/U^{6+} and M^{3+}/U^{5+} couples and magnetic susceptibility data show paramagnetic moments that are intermediate between these two scenarios. This assignment is compatible with the complex magnetic features observed in the susceptibility of these compounds at temperatures below 125 K.

Double perovskites are of interest for a range of possible applications and Sr_2MgMoO_6 has been shown to perform well as an anode for operation in a fuel cell. A structural study of three compounds in the $Sr_2MgMoO_{6-\delta}$ series has shown that all compounds crystallise in the triclinic space group $I\bar{1}$. Unusually rather than showing tilting of the oxide octahedra around multiple axes the tilting is close to tetragonal in symmetry with rotation mainly around a single axis. Instead the low symmetry arises from distortion of the octahedral units.[9] The Mg^{2+} and Mo^{6+} cations are almost perfectly ordered in a rock salt array across the oxide octahedra. The oxide non-stoichiometry, up to a value of $\delta = 0.046$, is correlated with the degree of cation mixing across the octahedral sites and this suggests that the formation of oxide vacancies is limited by the difficulty of forming five-coordinate Mg^{2+}.

A study of the $Sc_{1-x}Lu_xVO_3$ system has shown that Lu-rich compounds ($x > 0.58$) form distorted perovskites with the $GdFeO_3$ structure, whilst the Sc-rich compounds ($x < 0.1$) adopt the bixbyite structure that can be derived from the anion-deficient fluorite structure.[10] *In situ* diffraction experiments show that these bixbyite phases are metastable and further heating leads to formation of a mixture of bixbyite and a Lu-rich perovskite phase followed by cation exchange between these two phases leading to Lu- and Sc-enrichment of the perovskite and bixbyite phases, respectively. This insight has allowed the preparation of single phase bixbyite phases that are thermodynamically unstable.

A careful single crystal diffraction study has identified the structure of $Ba_{11}W_4O_{23}$ for the first time.[11] A compound of approximately this composition has been referred to in the literature over the last three decades but the structure has not been determined, but described as either perovskite or cryolite. The actual structure is derived from perovskite but contains two remarkable features (i) ordering of A-site vacancies and (ii) the same cation, Ba^{2+}, on both the A and B sites in the structure as indicated by the formulation $(Ba_{1.75}\square_{0.25})BaWO_{5.75}$. This complexity leads to a $4 \times 4 \times 4$ superstructure of the simple perovskite and a face centred lattice, $Fd\bar{3}m$, a = 17.1823(1) Å. The oxide sublattice shows considerable positional and occupational disorder leading to a mixture of octahedral and tetrahedral coordination environments around half of the W^{6+} cations.

The behaviour of vacancies in anion sublattices has been studied and led to the identification of a number of unusual new compounds. $Ba_7Mn_5Cr_2O_{20}$ can be derived from the simple ABO_3 stoichiometry by removal of 1/7 of the oxide anions from a 21-layer perovskite containing a mixture of hexagonal and cubic stacking of BaO_3 layers in a $(hhccc'cc)_3$ sequence. This leads to the formation of a BaO_2 layer denoted by c' and tetrahedral coordination environments for 2/7 of the transition metals.[12] This apparently small adjustment in stoichiometry has a profound effect on the oxidation states of the cations; the tetrahedra are almost entirely occupied by Cr^{2+} with the different octahedral sites occupied by Mn^{2+} and Mn^{4+} in a fully ordered arrangement as shown in Fig. 3. As well as showing a highly unusual

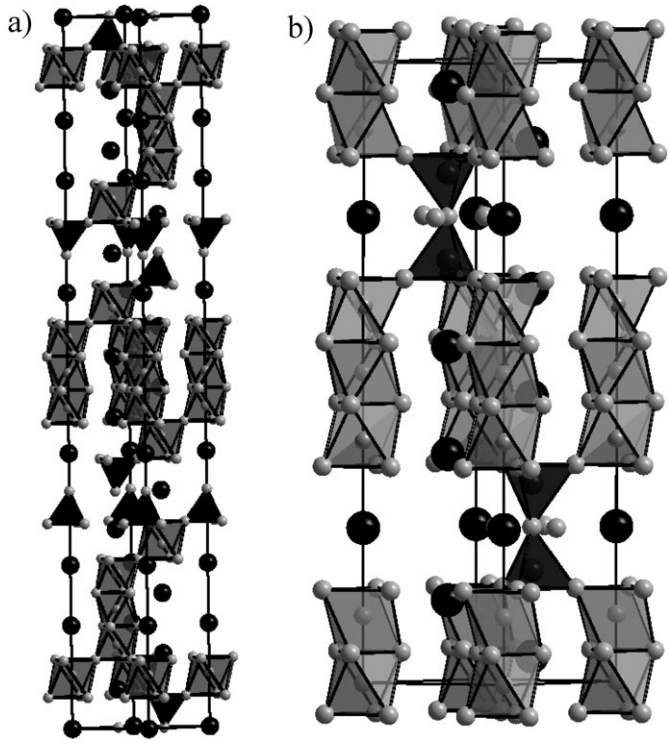

Fig. 3 (a) The 21R structure[12] of $Ba_7Mn_5Cr_2O_{20}$ and (b) the 10H structure[14] of $BaMn_{0.4}Fe_{0.6}O_{2.73}$. Spheres represent Ba^{2+} and polyhedra represent transition metal oxide units.

disproportionation of Mn^{3+} in the solid state this compound also demonstrates an elegant proof of the ability of anion deficiency to strongly direct the ordering of transition metal cations, a crucial process in tailoring the physical properties of new materials. The isostructural compound $Ba_7Y_2Mn_3Ti_2O_{20}$ contains Y^{3+} on a corner-sharing octahedral site with Mn^{4+} and Ti^{4+} distributed over the remaining face-sharing octahedral and tetrahedral sites.[13] There is considerable positional disorder in the oxide-deficient layer associated with the tetrahedrally-coordinated interstice suggesting that this portion of the structure is responsible for the observed oxide anion mobility. Organisation of hexagonal and cubic stacking in a $(hch'ch)_2$ arrangement gives the 10H structure observed in $BaMn_{0.4}Fe_{0.6}O_{2.73}$.[14] The cations are distributed over all three sites in the structure, although Mn shows a preference for the central octahedron of the face-sharing trimer whilst Fe favours the positions located adjacent to the anion deficient layer. The presence of Mn in the latter position favours the formation of face-sharing octahedra, rather than the tetrahedral coordination preferred by Fe and this leads to considerable disorder in the oxide anion position in the h' layer as shown in Fig. 3. This material is an insulator with a low activation energy suggesting a polaron hopping mechanism for conductivity.

A mixture of octahedral and tetrahedral coordination environments is also found in $Ba_2Co_9O_{14}$.[15] This structure is derived from the stacking of O_4 and BaO_3 layers leading to layers of edge-sharing CoO_6 octahedra linked by trimers of face-sharing CoO_6 octahedra which are themselves linked by corner-sharing CoO_4 tetrahedral

units. The face-sharing octahedra are occupied by low-spin Co^{3+}, whilst the tetrahedra contain Co^{2+} and the cations in the edge-shared CoO_6 layer are populated by an ordered arrangement of Co^{3+} and Co^{2+}. This complex distribution of paramagnetic cations leads to antiferromagnetic order, $T_N = 39$ K, with magnetic moments of 1.7 and 2.8 μ_B for the tetrahedrally- and octahedrally-coordinated Co, respectively.

The treatment of $SrFeO_{2.875}$ with the reducing agent CaH_2 at 300 °C has produced the remarkable Fe^{2+} compound $SrFeO_2$.[16] This compound is isostructural with $SrCuO_2$ and crystallises in the space group $P4/mmm$ [$a = 3.926$, $c = 3.432$ Å]. This strong deviation from the cubic symmetry of the parent structure arises from the ordering of the anion vacancies, disrupting the three-dimensional connectivity of the perovskite structure to give a layered phase consisting of corner sharing square-planar FeO_4. This material contains high spin Fe^{2+} ($S = 2$) aligned antiferromagnetically below a Néel temperature of 473 K. Despite the largely 2-dimensional nature of the magnetic interactions, the magnetic ordering temperature in this compound is considerably higher than other Fe^{2+} compounds such as FeO, $T_N \approx 200$ K. It is also noteworthy that the doubly degenerate $(d_{xz}, d_{yz})^3$ ground state does not lead to Jahn–Teller instability. Control of the reaction temperature leads to varying degrees of reduction of the $SrFeO_{3-\delta}$ phases. These reactions are not simply topotactic but involve rearrangement of the anion sublattice and it is remarkable that these reductions, and re-oxidations, can take place at temperatures as low 120 °C indicative of highly mobile oxide anions which nevertheless do not lead to phase separation or any appreciable loss of crystallinity. Low temperatures have also been used to stabilise unusually low oxidation states in the layered compounds $La_4Ni_3O_8$ and $Nd_4Ni_3O_8$.[17] These compounds were prepared by heating the $n = 3$ Ruddlesden–Popper phases $Ln_4Ni_3O_{10}$ under hydrogen at *ca.* 330 °C. These phases are composed of an intergrowth of the LnO_2 fluorite layers with triple-layers of $LnNiO_2$ containing a mixture of mono- and di-valent Ni that show clear similarities with the square planar arrangement of Fe^{2+} observed in $SrFeO_2$.

Anion deficiency in the pyrochlore structure is found in $RbOs_2O_6$ which contains Rb^+ on the vacated anion position to give the β-pyrochlore structure.[18] This site has six Rb–O distances of 3.114 Å and a further 12 Rb–O distances of 3.623 Å. These weak interactions lead to loosely bound Rb^+ which is reflected in the five-fold increase in the observed displacement of this cation on heating from 2 K to room temperature. Due to the size of the site, these displacements have minimal impact on the size of the unit cell and the $Fd\bar{3}m$ space group is preserved throughout this temperature range.

The complex oxides $Nd_{14}Na_3Ru_6O_{36}$ and $Pr_{14}Na_3Ru_6O_{36}$ are isostructural and crystallise in the space group $R\bar{3}c$ [$a = 9.7380$, $c = 55.5716$ Å for the Nd compound].[19] These compounds contain a complex distribution of Na and Ru in a number of trigonal prismatically- and octahedrally-coordinated sites, respectively. The RuO_6 octahedra are found in the middle of a face sharing $[Na_2RuO_{12}]$ unit as well as RuO_6 octahedra that are isolated by linkages to 8-coordinate Nd or Pr. The oxide octahedra are equally occupied by Ru^{4+} and Ru^{5+} in a fully ordered arrangement. Both compounds contain antiferromagnetic coupling in the paramagnetic regime but cooling below 10 K (8 K for $Pr_{14}Na_3Ru_6O_{36}$) $Nd_{14}Na_3Ru_6O_{36}$ develops an uncompensated magnetic moment develops indicative of canted antiferromagnetic, or ferrimagnetic ordering.

A number of new lithium-containing garnets have been reported.[20,21] The introduction of Zr^{4+} into these family of compounds has led to the formation of

$Li_7La_3Zr_2TaO_{12}$ which shows a total Li^+ conductivity of $\sigma = 3 \times 10^{-4}$ S cm^{-1} at room temperature.[22] The structure of such lithium-stuffed garnets has been studied in the $Li_{5+x}Ba_xLa_{3-x}Ta_2O_{12}$ system up to a maximum value of $x = 1.6$.[23] This neutron diffraction study has identified the presence of majority occupation of both tetrahedrally- and octahedrally-coordinated lithium sites in the structure. This is significant because these sites are linked *via* a shared polyhedral face giving a short Li···Li distance of $\approx$ 2.4 Å suggesting that Li^+ mobility will involve considerable local strain and thus a cooperative mechanism for cation motion in the garnet structure.

2. Oxyanions

Hydrothermal syntheses have been used to prepare a number of polar framework solids containing cations with d^0 and d^{10} electronic configurations to favour second harmonic generation. $(NH_4)_2Te_2WO_8$ forms a 2-dimensional structure by linking WO_6 octahedra and TeO_4 tetrahedra into layers separated by NH_4^+ cations.[24] The presence of d^0 and d^{10} configurations of W^{6+} and Te^{4+}, respectively leads to the asymmetric distortion of the environments around these cations due to second-order Jahn–Teller (SOJT) effects. These displacements are propagated through the lattice leading to the crystallisation in the noncentrosymmetric polar space group $P2_1$. The polarisation of the TeO_4 tetrahedra is partially cancelled, but a switchable polarisation of this material is clearly evident from hysteresis in the ferroelectric measurements. This material also shows a second harmonic generation of 250 times that of α-SiO_2. A similar rationale has lead to the study of the compounds $TlSeVO_5$ and $TlTeVO_5$ in which all three cations introduce SOJT effects.[25] These compounds again crystallise in a noncentrosymmetric polar space group ($Pna2_1$) and although both compounds form three-dimensional structures the connectivity between the VO_6 octahedra, SeO_3 or TeO_4 units and TlO_8 square antiprisms is different in the two structures. Despite these structural differences the physical properties of these compounds are similar with second harmonic generation, pyroelectricity and a non-switchable polarisation observed in both materials.

A new polymorph of $NaYSi_2O_6$ has been identified by quenching a high pressure reaction to ambient conditions.[26] The structure of this new phase is based on a three-membered ring composed of edge-sharing SiO_4 tetrahedral units arranged into corrugated layers separated by the cations. The formation of these $[Si_3O_9]^{12-}$ units is unusual due to the strain introduced into the structure as reflected by the low values (120–124°) of the Si–O–Si bond angles. High pressure conditions (7.5 GPa) have also lead to the first crystalline tin borate; materials in the Sn–B–O composition system commonly form glasses. The compound β-SnB_4O_7 is isotypic with a number of existing borates and forms a three-dimensional structure from corner-sharing BO_4 tetrahedra yielding unidirectional channels that accommodate Sn^{2+} in a coordination environment that is considerably modified from the isotypic phases by the presence of the sterically active $5s^2$ lone pair of Sn^{2+}.[27] Any insight into the structural chemistry of the tin borate phases is likely to be important in understanding the exceptional lithium intercalation properties of tin-based amorphous composite materials. Unusual coordination has been found in the new aluminoborate $HAl_2B_3O_8$ which contains Al exclusively in an exceptional 5-coordinate square-based pyramidal environment.[28]

A number of studies have incorporated a range of paramagnetic species into the framework materials. Three new amine-templated uranium phosphites have been

reported that show uranium is coordinated by a mixture of fluoride and oxide.[29] Two of the structures feature edge-sharing $U(O/F)_8$ polyhedra that are bridged by HPO_3 units suggesting that this cluster may be considered as a building unit in the design of new uranium framework materials. Magnetic measurements show the presence of antiferromagnetic interactions in a complex magnetic system and spectroscopic measurements show emission indicating upconversion arising from two photon absorption. A novel metal phosphoxalate has been prepared by protonating the amine commonly used as a template and incorporation of Na^+ from the sodium oxalate reagent.[30] This has yielded a 3-dimensional structure composed of layers of $[Co(C_2O_4)]$ linked by bidentate HPO_4^{2-} with the $H_3N^+CH_2CH_2N^+H_3$ and Na^+ cations found within different channels in the structure. The absence of analogous materials based on other alkali metals leads to the deduction that Na^+ acts as a structure-directing agent during phase formation.

An extensive survey of iron arsenate chemistry has identified six new framework materials.[31] As well as the relatively dense materials $Fe_2As_2O_7 \cdot 2H_2O$ and $LiFeAsO_4OH$, the use of diamines led to the formation of structures in which the doubly protonated amines occupy non-framework volume. The frameworks are composed of FeO_6 octahedra and tetrahedra of partially protonated $As(O,OH)_4$ units which provide a contrast to the analogous phosphate chemistry where protonation is not observed. In $LiFeAsO_4OH$ the framework charge is balanced by extra-framework Li^+. Extra framework Li^+ is a crucial component in the formation of the new phase $Li_4VO(PO_4)_2$.[32] This compound was synthesised from the proton conductor $VO(H_2PO_4)_2$ using treatment with LiBr solution to effect a topotactic reduction. $Li_4VO(PO_4)_2$ retains the $V_2P_2O_{15}$ chains of the parent material but disrupts the bonding between these chains leading to the conversion from a 3D proton conductor to a layered arrangement of Li^+ in $Li_4VO(PO_4)_2$. This compound shows reasonable lithium mobility ($\sigma = 10^{-4}$ S cm^{-1} at 550 °C) which is anticipated to be highly anisotropic.

The new potassium gallosilicate zeolite $K_{8.2}Ga_{8.2}Si_{11.8}O_{40} \cdot 11.5H_2O$ also shows remarkable guest properties.[33] The as-synthesised material has the natrolite topology and retains structural integrity in the temperature range $50 \leq T/K \leq 300$ with the orthorhombic space group $I2_12_12_1$. Heating the material above this temperature leads to partial loss of water and associated structural transformation to tetragonal symmetry, $I\bar{4}2d$. Increasing the temperature further leads to complete loss of water and a reduction in volume of 15%. Exposure to damp air at ambient conditions shows that these processes are fully reversible. This is the first observation of a dehydration-induced order-disorder transition in a zeolite and given the continuous 3-dimensional network of corner sharing $Si(Ga)O_4$ tetrahedra in these compounds this study demonstrates an remarkable flexibility in the zeolite framework.

The siliceous zeolite IM-5 has high thermal stability and is used for hydrocarbon cracking and reduction of NO. However, the application of this important material has been hampered by a lack of knowledge of it's structure; the pore structure has been mapped by a range of test reactions but the complexity of the structure, and higher metric symmetry, have posed a long-standing challenge to solving the structure using diffraction from material that is only available in polycrystalline form. The development of a new algorithm combining X-ray diffraction data with electron microscopy data has permitted the elucidation of this structure for the first time.[34] Given the difficulties inherent to the structure, combined with problems of sample purity and peak broadening, the incorporation of the more local probe of the

electron microscope has been crucial in indexing the X-ray diffraction peaks arising from the target phase. The refined structure contains 24 topologically distinct Si atoms, making it the most complex zeolite structure solved to date. Whilst the pore system has some features common to other zeolites, it is unusual in containing 10 ring channels which are partially interconnected. This gives large voids at the intersections of these channels which may permit the formation of large intermediate species, but the overall pore structure remains 2-dimensional in nature.

The new all-silica zeolite SSZ-73, isostructural with the aluminophosphate STA-6, has been prepared from fluoride-containing gels by using a polycyclic structure directing agent (SDA).[35] Although the unidirectional channels in this structure are composed of 8-ring pores the micropore volume of 0.25 g cm^{-3} is considerably larger than either 2-dimensional 8-ring or 1-dimensional 10-ring pore systems. Although the F^- anion could be located in the structural refinement, the weak interaction between the cationic SDA and the neutral framework meant that positional disorder prevented refinement of the coordinates of this positively charged guest. The use of a much smaller SDA, ($H_3NC_3H_7$), has resulted in the formation of much larger pores in a new germanate containing a 3-dimensional arrangement of 16- and 14-ring pores.[36] The negatively-charged framework is build up from a mixture of corner- and edge-sharing oxide polyhedra containing Ge in tetrahedral, square pyramidal and trigonal bipyramidal coordination environments. These give $[Ge_9O_{22}OH)_3]$ units that are linked by bridging oxide anions to give the framework shown in Fig. 4. The water can be removed from the channels of the structure to give a porous

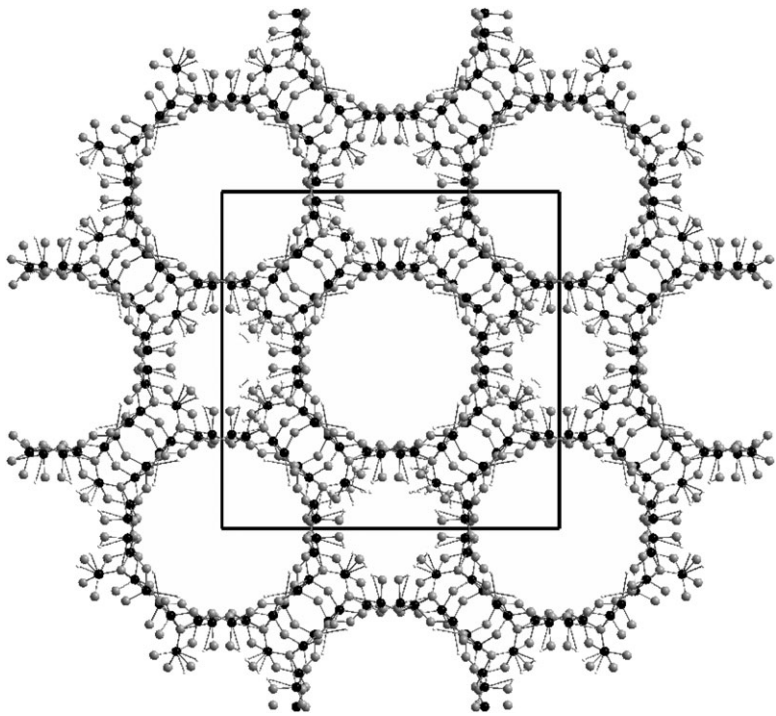

Fig. 4 The framework structure of $(H_3NC_3H_7)_5(H_3O)[Ge_{18}O_{36}(OH)_6]\cdot 3H_2O$ viewed along [001] in order to show the 16-ring channels.[36] Ge and O are represented by black and grey spheres, respectively. Non-framework atoms have been removed for clarity.

structure, but removal of the charge-compensating cations from the extra framework volume leads to structural collapse.

Exceptionally large channels formed from the coiling of a net containing 10-ring apertures have been reported in a new metal phosphate.[37] These 1-dimensional 24-ring channels are linked by 10-ring windows to give a 3-dimensional pore system with a diameters, $\leq$16 Å, that are significantly larger than observed in structurally related systems that also feature 24-ring channels.

3. Chalcogenides

The electronic properties of the series $Ga_x(V_{4-y}Cr_y)S_8$ have been studied in detail to examine the effect of electron doping on the ferromagnet GaV_4S_8.[38] For doping levels up to $y = 1.5$ the $GaMo_4S_8$ structure containing the tetrahedral V/Cr clusters shown in Fig. 5 is maintained. For higher levels of Cr-doping additional gallium is introduced into another tetrahedral site leading to rapid expansion of the lattice, the disruption of the V/Cr clusters and the formation of spinel phases. Spinel formation occurs for two reasons; it avoids the spin pairing that would be necessary if the $GaMo_4S_8$ structure were maintained at high Cr-doping levels and it is favoured by the stability of the Cr^{3+} in sulfides.

High ion mobility has been exploited in two systems to access new compounds by topotactic insertion. The 3-dimensional structure of Mo_2SbS_2 has been modified by reaction with lithium in order to evaluate the effect of reductive intercalation on the superconductivity that has been reported for the parent phase.[39] The structures of the resultant series $Li_xMo_2SbS_2$ ($0 \leq x \leq 0.7$) contain $[MoSbS]_\infty$ layers linked by chains of $[MoS]_\infty$ as shown in Fig. 6. In both of these units the Mo is in the 6-coordinated octahedral units MoS_3Sb_3 and MoS_4Sb_2 that compose the layers and

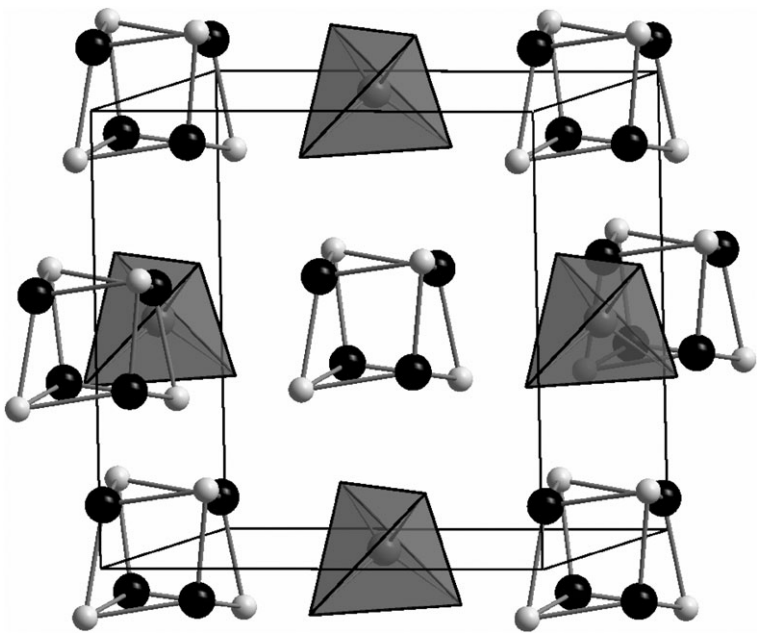

Fig. 5 The structure of $GaV_{4-x}Cr_xS_8$.[38] Tetrahedra represent GaS_4^{5-} units and V (black) and S (grey) form $V_4S_4^{5+}$ cubes.

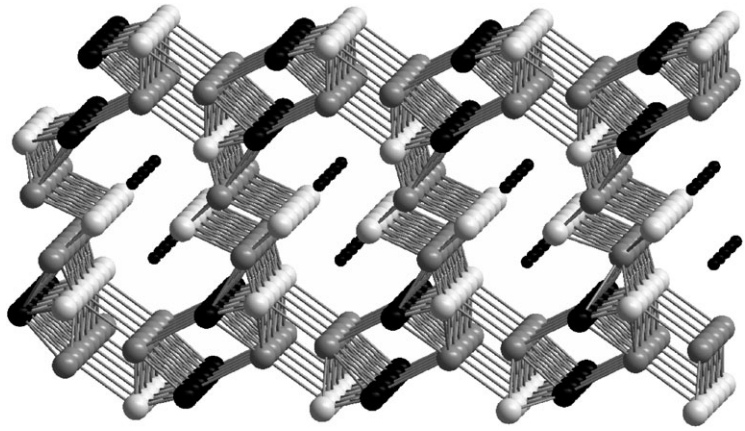

Fig. 6 The structure of the phases $Li_xMo_2SbS_2$.[39] The framework is composed of Mo, Sb and S that are shown as dark grey, black and light grey spheres, respectively. The intercalated Li is shown as small black spheres occupying the channels in the structure.

chains, respectively. Intercalation of Li leads to population of tetrahedral interstices that were previously vacant and anisotropic expansion of the lattice. This electron doping has a modest impact on the properties of the host structure and metallic behaviour is observed for all compositions; superconductivity could not be induced by application of pressures up to 17 kbar. Calculations show that this weak effect is, in part, due to localisation of carriers around the lattice distortions found at the Mo and Li sites.

The phases $Sr_4Mn_3O_{7.5}Cu_2Q_2$ (Q = S, Se) can be described as intergrowths of $Sr_4Mn_3O_{8-\delta}$ slabs of the perovskite structure with anti-fluorite layers composed of Cu_2Q_2. These materials can be fluorinated by reaction with XeF_2 or reduced by reaction with NaH.[40] The former leads to oxidation and the incorporation of additional anions into the structure giving stoichiometries such as $Sr_4Mn_{2.77}O_{7.27}F_{0.29}Cu_2S_2$ whilst reaction of the same starting material with NaH gives a phase of composition $Sr_4Mn_{2.77}O_{7.16}Cu_2S_2$. The magnetic properties of these materials are highly sensitive to these structural adjustments. The Ruddlesden-Popper phases $La_2LnMS_2O_5$ (Ln = La, Y; M = Nb, Ta) also contain perovskite slabs but these layers are separated by layers of rock-salt structured slabs of La_2S_2. The perovskite slabs in these materials are unusual in that they contain M and Ln in a disordered arrangement in the oxide octahedra, whilst the central interstice commonly occupied by relatively large cations remains vacant. This vacant site can be partially occupied by iodide; heating a reaction mixture of the composition $La_4Nb_2S_4O_7$ with iodine led to a highly unusual population of this site in a compound of stoichiometry $La_{2.89}Nb_{1.11}S_2O_5I_{0.22}$.[41]

The search for new thermoelectric materials has led to the preparation of new, isostructural chalcogenides $Ni_3Cr_2P_2Q_9$ (Q = S, Se).[42] These compounds contain $(Ni,Cr)Se_6$ octahedra that are linked *via* edges to give the honeycomb structure shown in Fig. 7. These layers are paired by shared octahedral faces and contain linear P-M-P units in the holes of the honeycomb, leading to each of these ions being coordinated to 3 chalcogenide anions. Transport measurements identified *p*-type conductivity with activation energies of 0.02–0.03 eV for the mixed anion phases and show that the composition $Ni_3Cr_2P_2S_6Se_3$ has reasonable thermopower. However,

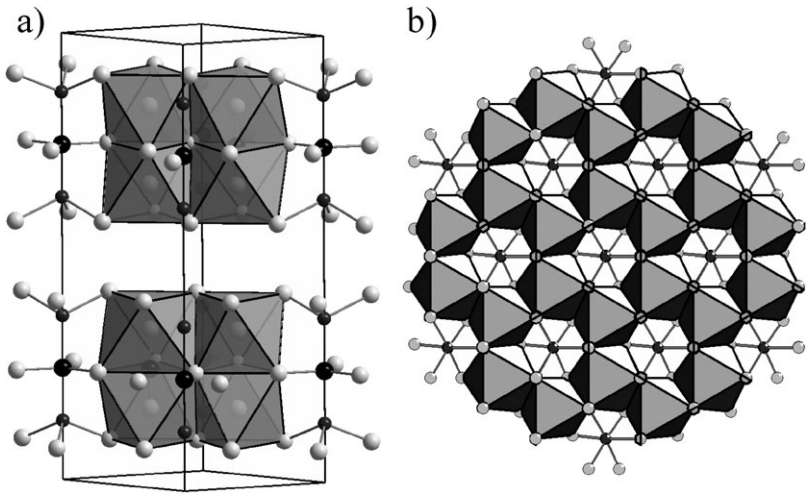

Fig. 7 (a) The structure of the $Ni_3Cr_2P_2S_{9x}Se_x$.[42] Octahedra represent CrO_6 units, Ni and P are shown as black and dark grey spheres, respectively and the chalcogenide atoms are represented by light grey spheres. (b) Shows the arrangement of CrO_6 octahedra and Ni within a single layer.

the high resistivity of these compounds mean that these materials will not be suitable for applications and that doping is unlikely to produce a useful *p*-type thermoelectric material. The new thiotellurate Tl_2TeS_3 has a large direct band gap of 1.61 eV but a smaller indirect bandgap of 0.9 eV that suggests that it may provide a basis for doping to yield new thermoelectric materials.[43] The structure of this compound can be described as containing layers of face-sharing Tl_8 cubes that each contain a trigonal pyramidal TeS_3^{2-} anion. These layers are stacked in an AABB arrangement. The structural similarities with alkali metal-containing analogues and the band gap measurements suggest that Tl^+ offers some advantages as a dopant in these materials and calculations show that any distortions induced by the presence of the $6s^2$ lone pair are likely to be smaller in sulfur compounds than those found in oxide chemistry.

The mixed lanthanide sulfides δ-$Ln_{2-x}Lu_xS_3$ (*Ln* = Ce, Pr, Nd) crystallise with the complex 3-dimensional structure previously reported for $CeTmS_3$.[44] It contains Ln^{3+} on 9-, 8-, and 7-coordinate sites. The 7-coordinate positions are partly occupied with Lu^{3+} in a disordered arrangement and this cation is also found in 6-coordination. Optical measurements show that these compounds are wide band-gap semiconductors. These compounds do not contain any S–S bonding and so the oxidation states of the different ions can be readily assigned. A study of the effects of doping on the $K_4Nb_2S_{11}$ structure has yielded five new compounds which show varying degrees of S–S bonding. This leads to a diverse range of structures where the complexity of the anion ranges from $[MS_4]^{3-}$ tetrahedra (found in $K_3V_{0.32}Ta_{0.68}S_4$) to $[M_4S_{25}]^{6-}$ found in $K_6Nb_{2.97}Ta_{1.03}S_{25}$.[45] Other stoichiometries lead to the formation of 1- and 2-dimensional frameworks that are separated by K^+ and do not contain any S–S bonding.

The polar structure of CaZnOS has been identified for the first time and has led to a study of the electrical properties of this phase.[46] The structure consists of layers of $ZnOS_3$ tetrahedra linked *via* corner sharing between all three S^{2-} anions with Ca^{2+}

occupying distorted octahedral sites to give CaS_3O_3 units. This unusual structure is noncentrosymmetric, space group $P6_3mc$, and shows an efficiency for second harmonic generation of *ca.* 100 times greater than quartz. The crystal structure prevents the switching of the dipole moment and so no ferroelectricity is observed.

4. Halides, nitrides and intermetallics

There have been a number of new oxide fluoride compounds reported in 2007. The Aurivillius phase Bi_2NbO_5F contains layers of $Nb(O,F)_6$ octahedra separated by fluorite-like layer of $M_2(O,F)_2$.[47] Due to the similar scattering of both X-rays and neutrons from F^- and O^{2-} an analysis of the bond lengths is necessary to determine the anion distribution and this suggests that F^- occupies the apical positions in the octahedra giving a composition for the perovskite layer of NbO_5F. Dielectric measurements show no evidence for non-centrosymmetric or polar symmetry and on these observations suggest that the observed distortions of the anion sublattice occur in *Pbca*, rather than the polar space group $Pca2_1$ which is also capable of yielding a satisfactory fit to the neutron diffraction data.

Low dimensional structures are also reported for a series of V^{4+} oxide fluorides; $CsVOF_3$, $RbVOF_3$ and (*trans*-1,2-bis(4-pyridyl)ethylene)$[VOF_3]$.[48] A common feature of all three compounds is the formation of chains composed of corner-linking between *trans* oxide anions in the VOF_5 units. These chains are linked into pairs by a shared edge, with the oxide anion and the remaining fluoride bonded to a single V^{4+} centre. The magnetic properties of these materials reflect the anisotropic structure and show evidence of 1-dimensional antiferromagnetic coupling at relatively high temperatures but no clear indication of long-range magnetic ordering on cooling these materials to 2 K. The fluoride chemistry of V^{3+} has also revealed the presence of 1-dimensional units in another series of compounds.[49] In this case the chains are composed of VF_6 octahedra linked by *via* corner sharing in either a *cis* or *trans* fashion depending on the counter-cation. In the case of [4,4′-bipyridyl]$[VF_3]$ the chains of *trans*-linked VF_6 octahedra are cross-linked by 4,4′-bipyridyl to give a 2-dimensional network.

Fluorination of the anion deficient perovskite $BaFeO_{3-\delta}$ at 400 °C has yielded the new cubic perovskite $BaFeO_2F$.[50] The oxide and fluoride cations are disordered over a single crystallographic site and provide a sufficiently effective pathway for magnetic superexchange that this material is antiferromagnetically ordered below $T_N \approx 645$ K. It is possible that this synthetic route can be applied to other systems to produce new mixed-metal oxide fluorides. Consideration of the bonding arrangements of related anion-deficient perovskites in the $BaCoO_{3-\delta}$ system has identified a reaction for the insertion of fluoride into the 5H and 12H polytypes to give new compounds with stoichiometries $Ba_5Co_5FO_{13-\delta}$ and $Ba_6Co_6FO_{16-\delta}$, respectively.[51] These modifications change the stacking sequence of the layers in the structure and link together the transition metal polyhedra providing a facile method of modifying the electronic properties of these structures.

Unusual synthetic methods been used to produce new nitride materials, most strikingly $Ti_{3-\delta}O_4N$.[52] This compound was characterised from a thin film sample that was prepared by chemical vapour deposition from a mixture containing $TiCl_4$, ethyl acetate and NH_3. The arrangements for mixing the precursor gases provided combinatorial access to a wide range of deposition conditions in a single experiment. The structure of $Ti_{2.85}O_4N$ was determined by X-diffraction experiments carried out on *ca.* 15 mg of delaminated material. This compound contains Ti in two

crystallographically-distinct sites (TiO_5N and TiO_4N_2) with a mean oxidation state of +3.86. Both of these $Ti(O,N)_6$ octahedra are heavily distorted and the metal-deficiency is manifested in the form of vacancies on both sites. A new oxide nitride has been prepared by nitriding a precursor prepared from a citrate-based mixing of Ga and Li precursors.[53] The Li replaces Ga in the wurtzite structure and charge balance is maintained by replacement of nitride with oxide at the anion site to give a structure in which both the anion and cation sites are fully occupied, by a disordered arrangement of N/O and Li/Ga, respectively, to give a stoichiometry $Li_2Ga_3O_4N$.

The first ternary compound of the Ca/N/group 4 metal phase diagrams has been reported. Ca_4TiN_4, along with Ca_5NbN_5, was prepared by reaction in sealed niobium tubes using Li_3N as a flux.[54] Ca_4TiN_4 is isostructural with several oxides and contains a distorted TiN_4 tetrahedron with each of the 4 crystallographically distinct nitride anions forming a shared corner with polyhedral units that contain Ca in either 4- or 5-coordination. Ca_5NbN_5 forms a layered structure in which layers of edge-sharing CaN_6 octahedra alternate with layers composed of CaN_5 trigonal bipyramids and NbO_4 tetrahedra.

The first preparation of ReB_2 has been achieved by arc melting the component elements.[55] Incorporation of B into the interstitial sites of the Re lattice leads to only a 5% increase in the lattice parameter and gives a structure in which puckered hexagonal network of B alternates with layers of hexagonal close-packed Re that are found in the elemental metal. This covalent compound was targeted because it demonstrates a high valence electron density that leads to exceptional hardness; ReB_2 possesses an average hardness of 48 GPa that matches that of BN, and is second only to diamond (70–100 GPa). The remarkable mechanical properties of ReB_2 are of great practical interest as, unlike most superhard materials, it can be prepared under ambient pressure by simply heating Re and B powders in sealed quartz tube at 1000 °C for 5 days.

Flux growth of $YbAlB_4$ has identified the structure of a second polymorph that has not previously been observed.[56] $LuAlB_4$ is isostructural with β-$YbAlB_4$ and the lanthanide atoms and Al are found between B layers. The α- and β-$YbAlB_4$ structures differ in the arrangement of B within the layers, although this does not have a large impact on the Yb/Al distribution in the interlayer space. The magnetic susceptibility of these two polymorphs show similar variation with temperature and both phases show heavy fermion behaviour.

There are a number of In-rich compounds that also show heavy fermion behaviour and the development of liquid In as a reaction medium is anticipated to provide access to a range of compounds showing interesting electronic effects. Although the use of liquid In as a solvent has led to the formation of In-rich phases $LnAu_2In_4$ (Ln = La, Ce, Pr, Nd) the magnetic properties of these materials indicate that these materials are poor metals.[57] All of these compounds are isostructural and contain a $[Au_2In_4]^{3-}$ network containing channels that house the lanthanide atoms in an arrangement that provides bonds to eight In and four Au atoms. Electronic structure calculations indicate that a low density of states at the Fermi level is responsible for the weak magnetic interactions in these compounds. Interestingly the use of In as a solvent has also yielded compounds that are relatively In-poor; reaction in an excess of In has yielded the products $Ln_7Co_4InGe_{12}$ that provide the first examples of a new structure type.[58] These compounds again accommodate Ln within channels, although in these compounds the networks are composed of the 3-dimensional $[Co_4Ge_{12}]$ framework shown in Fig. 8. These compounds contain a

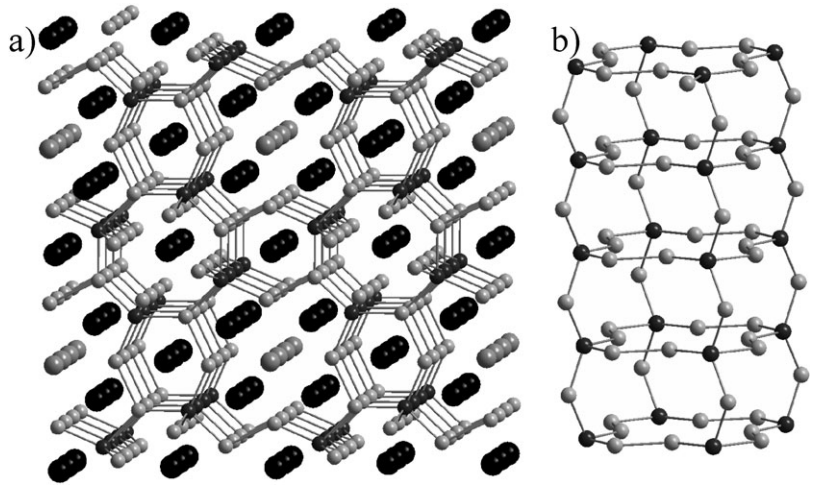

Fig. 8 The structure of $Ln_7Co_4InGe_{12}$.[58] (a) The framework is composed of Co (dark grey spheres) and Ge (light grey spheres). The bonding with the *Ln* (black spheres) and In (light grey spheres) is not shown. The 1-dimensional arrangement of the largest rings in the Co_4Ge_{12} framework is shown in (b) where the In and *Ln* atoms have been omitted for clarity.

mixture of Yb^{2+} and Yb^{3+} and show metallic conductivity and a weak negative magnetoresistance.

Metallic behaviour and a high density of states at the Fermi level leads to ferromagnetic ordering at temperature below $60 \leq T_C/K \leq 155$ for $LnCrGe_3$ (*Ln* = La, Pr, Nd, Sm).[59] These compounds all adopt the 2H hexagonal perovskite structure formed from the *AB* stacking of close packed layers of $LnGe_3$. This results in face sharing $CrGe_6$ octahedra and Cr···Cr separations of *ca.* 2.5 Å that suggest a weak bonding interaction between the Cr atoms. Despite the 1-dimensional appearance of the structure the presence of short Ge···Ge distances between the chains suggests the presence of single bonds between the Ge atoms and this provides an explanation of the relatively high temperature for the onset of 3-dimensional magnetic ordering in these materials.

A detailed examination of seven isostructural new phases from the compositional series $A_9Zn_{4+x}Pn_9$ and $A_9Cd_{4+x}Pn_9$ ($0 \leq x$ 0.5; *A* = Ca, Sr, Yb; *Pn* = Sb, Bi) has identified a subtle mechanism for non-stoichiometry that has previously been undetected.[60] This mechanism is most clearly evident in $Sr_9Cd_{4.49}Sb_9$. This compound contains Cd in the centre of tetrahedra composed of Sb and these units are linked together to give Cd_4Sb_9 ribbons with Sr occupying sites that are octahedrally-coordinated by six Sb atoms. The small stoichiometric variations in this structure are possible due to partial occupancy of an unusual trigonal prismatic environment by additional Cd atoms. Variations in stoichiometry introduce small departures from the ideal electron count and associated energetic penalties but these costs are compensated by the simultaneous adjustments in the crystal structure reducing the energy of the lattice. The authors conclude that the role of cations in the stability of Zintl phases can extend beyond acting as a provider of charge for the electronic structure.

The crystal structures of $Li_{33.3}Ba_{13.1}Ca_3$ and $Li_{18.9}Na_{8.3}Ba_{15.3}$ have been solved.[61] The former is described as a variant on the arsenic structure and the latter differs in

the arrangement of Na and Li. This variation in the non-Ba atomic distribution adds an additional layer of complexity to the structure and leads to a remarkably large unit cell, with a volume of 33 550 $Å^3$, that contains 158 crystallographically-unique metal sites. Known examples of Li–Na contacts are rare in the literature and the complex structure of $Li_{18.9}Na_{8.3}Ba_{15.3}$ means that this compound provides the first example of a very large number of such interactions.

References

1 E. E. Rodriguez, F. Poineau, A. Llobet, A. P. Sattelberger, J. Bhattacharjee, U. V. Waghmare, T. Hartmann and A. K. Cheetham, *J. Am. Chem. Soc.*, 2007, **129**, 10244.
2 H. L. Cuthbert, J. E. Greedan, I. Vargas-Baca, S. Derakhshan and I. P. Swainson, *Inorg. Chem.*, 2007, **46**, 8739.
3 N. V. Tarakina, E. A. Nikulina, J. Hadermann, D. G. Kellerman, A. P. Tyutyunnik, I. F. Berger, V. G. Zubkov and G. V. Tendeloo, *J. Solid State Chem.*, 2007, **180**, 3180.
4 G. King, S. Thimmaiah, A. Dwivedi and P. M. Woodward, *Chem. Mater.*, 2007, **19**, 6451.
5 Q. Zhou, B. J. Kennedy, M. M. Elcombe and R. L. Withers, *J. Solid State Chem.*, 2007, **180**, 3082.
6 E. J. Cussen, *J. Solid State Chem.*, 2007, **180**, 474.
7 M. Retuerto, M. Garcia-Hernandez, M. J. Martinez-Lopez, M. T. Fernandez-Diaz, J. P. Attfield and J. A. Alonso, *J. Mater. Chem.*, 2007, **17**, 3555.
8 R. M. Pinacca, M. C. Viola, J. C. Pedregosa, M. J. Martínez-Lope, R. E. Carbonio and J. A. Alonso, *J. Solid State Chem.*, 2007, **180**, 1582.
9 C. Bernuy-Lopez, M. Allix, C. A. Bridges, J. B. Claridge and M. J. Rosseinsky, *Chem. Mater.*, 2007, **19**, 1035.
10 R. J. Lundgren, L. M. D. Cranswick and M. Bieringer, *Chem. Mater.*, 2007, **19**, 3945.
11 S.-T. Hong, *J. Solid State Chem.*, 2007, **180**, 3039.
12 S. J. Dunstone, J. H. Clark and M. A. Hayward, *Chem. Commun.*, 2007, 1905.
13 X. Kuang, M. Allix, R. M. Ibberson, J. B. Claridge, H. Niu and M. J. Rosseinsky, *Chem. Mater.*, 2007, **19**, 2884.
14 L. Miranda, K. Boulahya, A. Varela, J. M. González-Calbet, M. Parras, M. Hernando, M. T. F.-D.A. Feteira and D. C. Sinclair, *Chem. Mater.*, 2007, **19**, 3425.
15 G. Ehora, S. Daviero-Minaud, M. Colmont, G. André and O. Mentré, *Chem. Mater.*, 2007, **19**, 2180.
16 Y. Tsujimoto, C. Tassel, N. Hayashi, T. Watanabe, H. Kageyama, K. Yoshimura, M. Takano, M. Ceretti, C. Ritter and W. Paulus, *Nature*, 2007, **450**, 1062.
17 V. V. Poltavets, K. A. Lokshin, M. Croft, T. K. Mandal, T. Egami and M. Greenblatt, *Inorg. Chem.*, 2007, **46**, 10887.
18 R. Galati, R. W. Hughes, C. S. Knee, P. F. Henry and M. T. Weller, *J. Mater. Chem.*, 2007, **17**, 160.
19 W. R. Gemmill, M. D. Smith and H. C. zur Loye, *Inorg. Chem.*, 2007, **46**, 2132.
20 E. J. Cussen and T. W. S. Yip, *J. Solid State Chem.*, 2007, **180**, 1832.
21 J. Percival and P. R. Slater, *Solid State Commun.*, 2007, **142**, 355.
22 R. Murugan, V. Thangadurai and W. Weppner, *Angew. Chem., Int. Ed.*, 2007, **46**, 7778.
23 M. P. O'Callaghan and E. J. Cussen, *Chem. Commun.*, 2007, 2048.
24 J. H. Kim, J. Baek and P. S. Halasyamani, *Chem. Mater.*, 2007, **19**, 5637.
25 T. Sivakurnar, H. Y. Chang, J. Baek and P. S. Halasyamani, *Chem. Mater.*, 2007, **19**, 4710.
26 V. Kahlenberg, J. Konzett and R. Kaindl, *J. Solid State Chem.*, 2007, **180**, 1934.
27 J. S. Knyrim, F. M. Schappacher, R. Pöttgen, J. S. auf der Günne, D. Johrendt and H. Huppertz, *Chem. Mater.*, 2007, **19**, 254.
28 T. Yang, J. Ju, G. Li, F. Liao, X. Zou, F. Deng, L. Chen, Y. Wang and J. Lin, *Inorg. Chem.*, 2007, **46**, 4772.
29 S. Mandal, M. Chandra and S. Natarajan, *Inorg. Chem.*, 2007, **46**, 7935.
30 T. Huang, B. A. Vanchura, Y. Shan and S. D. Huang, *J. Solid State Chem.*, 2007, **180**, 2110.
31 S. B. Wiggin, R. W. Hughes, D. J. Price and M. T. Weller, *Dalton Trans.*, 2007, 2935.
32 V. Caignaert, M. S. Kishore, V. Pralong, B. Raveau, N. Creon and H. Fjellväg, *J. Solid State Chem.*, 2007, **180**, 2437.
33 Y. Lee, S. J. Kim, I. Bull, A. J. Celestian, J. B. Parise, C. C. Kao and T. Vogt, *J. Am. Chem. Soc.*, 2007, **129**, 13744.
34 C. Baerlocher, F. Gramm, L. Massuger, L. B. McCusker, Z. B. He, S. Hovmoller and X. D. Zou, *Science*, 2007, **315**, 1113.

35 D. S. Wragg, R. Morris, A. W. Burton, S. I. Zones, K. Ong and G. Lee, *Chem. Mater.*, 2007, **19**, 3924.
36 M. P. Attfield, Y. Al-Ebini, R. G. Pritchard, E. M. Andrews, R. J. Charlesworth, W. Hung, B. J. Masheder and D. S. Royal, *Chem. Mater.*, 2007, **19**, 316.
37 Y. Yang, N. Li, H. Song, H. Wang, W. Chen and S. Xiang, *Chem. Mater.*, 2007, **19**, 1889.
38 D. Bichler and D. Johrendt, *Chem. Mater.*, 2007, **19**, 4316.
39 A. Lappas, C. J. Nuttall, Z. G. Fthenakis, V. Y. Pomjakushin and M. A. Roberts, *Chem. Mater.*, 2007, **19**, 69.
40 G. Hyett, N. Barrier, S. J. Clarke and J. Hadermann, *J. Am. Chem. Soc.*, 2007, **129**, 11192.
41 L. Cario, A. F. Popa, A. Lafond, C. Guillot-Deudon, H. Kabbour, A. Meerschaut, S. J. Clarke and P. Adamson, *Inorg. Chem.*, 2007, **46**, 9584.
42 M. A. McGuire and F. J. DiSalvo, *Chem. Mater.*, 2007, **19**, 4600.
43 F. Rieger and A.-V. Mudring, *Chem. Mater.*, 2007, **19**, 221.
44 G. B. Jin, E. S. Choi, R. P. Guertin, J. S. Brooks, T. H. Bray, C. H. Booth and T. E. Albrecht-Schmitt, *J. Solid State Chem.*, 2007, **180**, 2129.
45 Y. Wu and W. Bensch, *J. Solid State Chem.*, 2007, **180**, 2166.
46 T. Sambrook, C. F. Smura, S. J. Clarke, K. M. Ok and P. S. Halasyamani, *Inorg. Chem.*, 2007, **46**, 2571.
47 E. E. McCabe, I. P. Jones, D. Zhang, N. C. Hyatt and C. Greaves, *J. Mater. Chem.*, 2007, **17**, 1193.
48 D. W. Aldous, R. J. Goff, J. P. Attfield and P. Lightfoot, *Inorg. Chem.*, 2007, **46**, 1277.
49 D. W. Aldous, N. F. Stephens and P. Lightfoot, *Inorg. Chem. Commun.*, 2007, **46**, 3996.
50 R. Heap, P. R. Slater, F. J. Berry, O. Helgason and A. J. Wright, *Solid State Commun.*, 2007, **141**, 467.
51 G. Ehora, C. Renard, S. Daviero-Minaud and O. Mentré, *Chem. Mater.*, 2007, **19**, 2924.
52 G. Hyett, M. A. Green and I. P. Parkin, *J. Am. Chem. Soc.*, 2007, **129**, 15541.
53 S. Kikkawa, K. Nagasaka, T. Takeda, M. Bailey, T. Sakurai and Y. Miyamoto, *J. Solid State Chem.*, 2007, **180**, 1984.
54 J. L. Hunting, M. M. Szymanski, P. E. Johnson, C. B. Kellar and F. J. DiSalvo, *J. Solid State Chem.*, 2007, **180**, 31.
55 H. Y. Chung, M. B. Weinberger, J. B. Levine, R. W. Cumberland, A. Kavner, J. M. Yang, S. H. Tolbert and R. B. Kaner, *Science*, 2007, **317**, 750.
56 R. T. Macaluso, S. Nakatsuji, K. Kuga, E. L. Thomas, Y. Machida, Y. Maeno, Z. Fisk and J. Y. Chan, *Chem. Mater.*, 2007, **19**, 1918.
57 J. R. Salvador, K. Hoang, S. D. Mahanti and M. G. Kanatzidis, *Inorg. Chem.*, 2007, **46**, 6933.
58 M. Chondroudi, M. Balasubramanian, U. Welp, W. K. Kwok and M. G. Kanatzidis, *Chem. Mater.*, 2007, **19**, 4769.
59 H. Bie, O. Y. Zelinska, A. V. Tkachuk and A. Mar, *Chem. Mater.*, 2007, **19**, 4613.
60 S. Q. Xia and S. Bobev, *J. Am. Chem. Soc.*, 2007, **129**, 10011.
61 V. Smetana, V. Babizhetskyy, C. Hoch and A. Simon, *J. Solid State Chem.*, 2007, **180**, 3302.